On the Microstructural Modeling of Vascular Tissues

Estefania Peña

Abstract Accurate determination of the biomechanical implications of vascular surgeries or pathologies on patients requires developing patient-specific models of the organ or vessel under consideration. In this regard, combining the development of advanced constitutive laws that mimic the behaviour of the vascular tissue with advanced computer analysis provides a powerful tool for modelling vascular tissues on a patient-specific basis. Collagen is the most abundant protein in mammals and provides soft biological tissue, like the vasculature, with mechanical strength, stiffness and toughness. In several tissues there is a strong alignment of the collagen fibres with little dispersion in their orientation, but in other cases, such as the artery wall, there is significant dispersion in the orientation, which has a significant influence on the mechanical response. Proposed structure-based models was used by taking into account the spatial dispersion or waviness of collagen fiber directions. Vascular tissues exhibits simultaneously elastic and viscous material response. The rate-dependent material behavior of this kind of materials has been well-documented and quantified in the literature. Furthermore, non-physiological loads drive soft tissue to damage that may induce a strong reduction of the stiffness. In this chapter, we have provided a critical review of the fundamental aspects in modeling this kind of the materials. The application of these constitutive relationships in the context of vascular system has been presented.

E. Peña (✉)
Applied Mechanics and Bioengineering Group,
Aragón Institute of Engineering Research (I3A), University of Zaragoza,
María de Luna s/n, Edif. Betancourt, 50018 Zaragoza, Spain
e-mail: fany@unizar.es

E. Peña
Centro de Investigación Biomédica en Red en Bioingeniería, Biomateriales
y Nanomedicina (CIBER-BBN), Zaragoza, Spain

J.M.R.S. Tavares and R.M. Natal Jorge (eds.), *Computational and Experimental Biomedical Sciences: Methods and Applications*, Lecture Notes in Computational Vision and Biomechanics 21, DOI 10.1007/978-3-319-15799-3_2

1 Introduction

The arterial wall is composed of three distinct elements: the vascular smooth muscles (VSM) that form the cellular part of the vessel, and the extracellular matrix major components elastin and collagen. Collagen is the main load-bearing component within the tissue, while the elastin provides elasticity to the tissue. Identification of an appropriate strain energy function (SEF) is the preferred method to describe the complex nonlinear elastic properties of vascular tissues [31]. An ideal SEF should be based on histological analysis to provide a better description of wall deformation under load [33, 54]. Early SEFs were purely phenomenological functions where parameters involved in the mathematical expression are not physiological meaning [17, 56]. Later, structure-based or constituent-based SEF were developed, where the parameters means some physical and structural properties of the different components of the vessel wall [26, 63]. In several tissues there is a strong alignment of the collagen fibres with little dispersion in their orientation, but in other cases, such as the artery wall, there is significant dispersion in the orientation, which has a significant influence on the mechanical response. Proposed structure-based models was used by taking into account the spatial dispersion or distribution or waviness of collagen fiber directions [2, 23, 33, 58, 62].

Collagen is the most abundant protein in mammals and provides soft biological tissue, like the vasculature, with mechanical strength, stiffness and toughness. Roach and Burton suggested that collagen had a main impact on the mechanical properties of arterial tissue at higher strain levels, i.e. where mechanical failure is supposed to appear. Vascular tissues exhibits simultaneously elastic and viscous material response. The rate-dependent material behavior of this kind of materials has been well-documented and quantified in the literature [21, 27, 41]. Furthermore, non-physiological loads drive soft tissue to damage that may induce a strong reduction of the stiffness [19, 35, 39, 41]. Damage may arise from two possible mechanisms: tear or plastic deformation of the fibers, or biochemical degradation of the extracellular matrix from protease release associated with the observed cellular necrosis.

Since the main modelling effort in the literature has been on the passive response of arteries, this is also the concern of the major part of this chapter. Taken all this into account, this chapter is focused on the development of microstructural constitutive models for vascular tissues and organized as follows. In Sect. 2 the constitutive equations of anisotropic hyperelastic materials are reviewed. In Sect. 3, we present the elastic micro-structurally based models. Section 4 considered a microstructural anisotropic damage and softening model for vessel tissues. Finally, Sect. 5 includes some concluding remarks.

2 Hyperelastic Behavior

This section deals with the formulation of standard finite strain material models for soft biological tissues. To clarify the framework it is necessary to summarize the formulation of finite strain hyperelasticity in terms of invariants with uncoupled volumetric/deviatoric responses, first suggested by Flory [16], generalized in [52] and employed for anisotropic soft biological tissues in [26, 59] among others.

Let $\mathscr{B}_0 \subset \mathbb{E}^3$ be a reference or rather material configuration of a body of interest. The notation $\boldsymbol{\varphi} : \mathscr{B}_0 \times \mathscr{T} \rightarrow \mathscr{B}_t$ represents the one to one mapping, continuously differentiable, transforming a material point $\mathbf{X} \in \mathscr{B}_0$ to a position $\mathbf{x} = \boldsymbol{\varphi}(\mathbf{X}, t) \in \mathscr{B}_t \subset \mathbb{E}^3$, where $\mathscr{B}_t$ represents the deformed configuration at time $t \in \mathscr{T} \subset \mathbb{R}$. The mapping $\boldsymbol{\varphi}$ represents a motion of the body that establishes the trajectory of a given point when moving from its reference position $\mathbf{X}$ to $\mathbf{x}$. The two-point deformation gradient tensor is defined as $\mathbf{F}(\mathbf{X}, t) := \nabla_{\mathbf{X}} \boldsymbol{\varphi}(\mathbf{X}, t)$, with $J(\mathbf{X}) = \det(\mathbf{F}) > 0$ the local volume variation.

The direction of a fiber at a point $\mathbf{X} \in \mathscr{B}_0$ is defined by a unit vector field $\mathbf{m}_0(\mathbf{X})$, $|\mathbf{m}_0| = 1$. It is usually assumed that, under deformation, the fiber moves with the material points of the continuum body, that is, it follows an affine deformation. Therefore, the stretch λ of the fiber defined as the ratio between its lengths at the deformed and reference configurations can be expressed as

$$\lambda \mathbf{m}(\mathbf{x}, t) = \mathbf{F}(\mathbf{X}, t)\mathbf{m}_0(\mathbf{X}), \tag{1}$$

where $\mathbf{m}$ is the unit vector of the fiber in the deformed configuration and

$$\lambda^2 = \mathbf{m}_0 \cdot \mathbf{F}^T\mathbf{F} \cdot \mathbf{m}_0 = \mathbf{m}_0 \cdot \mathbf{C}\mathbf{m}_0 \tag{2}$$

stands for the stretch along the fiber direction at point $\mathbf{X}$ (Fig. 1). In (2) $\mathbf{C} = \mathbf{F}^T\mathbf{F}$ is the standard deformation gradient and the corresponding right Cauchy-Green strain measure. The introduced kinematics for one family of fibers can be applied to a second fiber family in an analogous manner. We shall denote a second preferred fiber orientation by the unit vector field $\mathbf{n}_0(\mathbf{X})$.

It is sometimes useful to consider the multiplicative decomposition of $\mathbf{F}$

$$\mathbf{F} := J^{1/3}\mathbf{I} \cdot \bar{\mathbf{F}}. \tag{3}$$

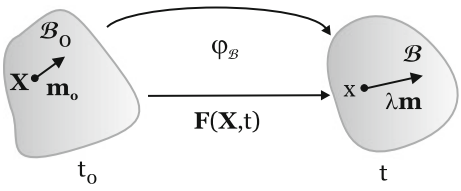

Fig. 1 Kinematics of a unit vector field $\mathbf{m}_0(\mathbf{X})$

Hence, deformation is split into a dilatational part, $J^{1/3}\mathbf{I}$, where $\mathbf{I}$ represents the second-order identity tensor, and an isochoric contribution, $\bar{\mathbf{F}}$, so that $\det(\bar{\mathbf{F}}) = 1$ [16]. With these quantities at hand, the isochoric counterparts of the right Cauchy-Green deformation tensors associated with $\bar{\mathbf{F}}$ are defined as $\bar{\mathbf{C}} := \bar{\mathbf{F}}^{\mathrm{T}} \cdot \bar{\mathbf{F}} = J^{-2/3}\mathbf{C}$.

The free energy function (SEF) is given by a scalar-valued function Ψ defined per unit reference volume in the reference configuration and for isothermal processes. Flory [16] postulated the additive decoupled representation of this SEF in volumetric and isochoric parts. To differentiate between the isotropic and the anisotropic parts, the free energy density function can be split up again as

$$\Psi = \Psi_{\mathrm{vol}} + \bar{\Psi} = \Psi_{\mathrm{vol}} + \bar{\Psi}_{\mathrm{iso}} + \bar{\Psi}_{\mathrm{ani}}, \tag{4}$$

where Ψ_{vol} describes the free energy associated to changes of volume, $\bar{\Psi}_{\mathrm{iso}}$ is the isochoric isotropic contribution of the free energy (usually associated to the ground matrix) and $\bar{\Psi}_{\mathrm{ani}}$ takes into account the isochoric anisotropic contribution (associated to the fibers) [55].

This strain-energy density function must satisfy the principle material frame invariance $\Psi(\mathbf{C}, \mathbf{M}, \mathbf{N}) = \Psi(\mathbf{Q} \cdot \mathbf{C}, \mathbf{Q} \cdot \mathbf{M}, \mathbf{Q} \cdot \mathbf{N})$ for all $[\mathbf{C}, \mathbf{Q}] \in \left[\mathbb{S}^3_+ \times \mathbb{Q}^3_+\right]$. Because of the directional dependence on the deformation, we require that the function Ψ explicitly depends on both the right Cauchy-Green tensor $\mathbf{C}$ and the fibers directions in the reference configuration ($\mathbf{m}_0$ and $\mathbf{n}_0$ in the case of two fiber families). Since the sign of $\mathbf{m}_0$ and $\mathbf{n}_0$ is not significant, Ψ must be an even function of $\mathbf{m}_0$ and $\mathbf{n}_0$ and so it may be expressed by $\Psi = \Psi(\mathbf{C}, \mathbf{M}, \mathbf{N})$ where $\mathbf{M} = \mathbf{m}_0 \otimes \mathbf{m}_0$ and $\mathbf{N} = \mathbf{n}_0 \otimes \mathbf{n}_0$ are structural tensors [55]. In terms of the strain invariants [55], Ψ can be written as

$$\Psi = \Psi_{\mathrm{vol}}(J) + \bar{\Psi}_{\mathrm{iso}}(\bar{I}_1, \bar{I}_2) + \bar{\Psi}_{\mathrm{ani}}(\bar{I}_4, \bar{I}_5, \bar{I}_6, \bar{I}_7, \bar{I}_8, \bar{I}_9) \tag{5}$$

with $\bar{I}_1$ and $\bar{I}_2$ the first two modified strain invariants of the symmetric modified Cauchy-Green tensor $\bar{\mathbf{C}}$ (note that $I_3 = J^2$). Finally, the anisotropic invariants $\bar{I}_4, \ldots, \bar{I}_9$ characterize the constitutive response of the fibers [55]:

$$\begin{aligned} \bar{I}_4 &= \bar{\mathbf{C}} : \mathbf{M} = \bar{\lambda}_m^2, \quad \bar{I}_5 = \bar{\mathbf{C}}^2 : \mathbf{M} \\ \bar{I}_6 &= \bar{\mathbf{C}} : \mathbf{N} = \bar{\lambda}_n^2, \quad \bar{I}_7 = \bar{\mathbf{C}}^2 : \mathbf{N} \\ \bar{I}_8 &= [\mathbf{m}_0 \cdot \mathbf{n}_0]\mathbf{m}_0 \cdot \bar{\mathbf{C}}\mathbf{n}_0 \quad \bar{I}_9 = [\mathbf{m}_0 \cdot \mathbf{n}_0]^2. \end{aligned} \tag{6}$$

Remark While the invariants $\bar{I}_4$ and $\bar{I}_6$ have a clear physical meaning, the square of the stretch λ in the fibers directions, the influence of $\bar{I}_5$, $\bar{I}_7$ and $\bar{I}_8$ is difficult to evaluate due to the high correlation between them [28]. For this reason and the lack of sufficient experimental data it is usual not to include these invariants in the definition of Ψ for soft biological tissues. Finally, $\bar{I}_9$ does not depend on the deformation.

The second Piola-Kirchhoff stress tensor is obtained by derivation of (4) with respect to the right Cauchy-Green tensor [37]. Thus, the stress tensor consists of a purely volumetric and a purely isochoric contribution, i.e. $\mathbf{S}_{\text{vol}}$ and $\bar{\mathbf{S}}$, so the total stress is

$$\begin{aligned}\mathbf{S} = \mathbf{S}_{\text{vol}} + \bar{\mathbf{S}} &= 2\frac{\partial \Psi_{\text{vol}}(J)}{\partial \mathbf{C}} + 2\frac{\partial \bar{\Psi}(\bar{\mathbf{C}}, \mathbf{M}, \mathbf{N})}{\partial \mathbf{C}} = \left[\frac{\partial \Psi_{\text{vol}}(J)}{\partial J}\frac{\partial J}{\partial \mathbf{C}} + \frac{\partial \bar{\Psi}(\bar{\mathbf{C}}, \mathbf{M}, \mathbf{N})}{\partial \bar{\mathbf{C}}}\frac{\partial \bar{\mathbf{C}}}{\partial \mathbf{C}}\right] \\ &= Jp\mathbf{C}^{-1} + \sum_{j=1,2,4,6} \mathsf{P} : 2\frac{\partial \bar{\Psi}}{\partial \bar{I}_j}\frac{\partial \bar{I}_j}{\partial \bar{\mathbf{C}}} = Jp\mathbf{C}^{-1} + \mathsf{P} : \tilde{\mathbf{S}},\end{aligned} \tag{7}$$

where the second Piola-Kirchhoff stress $\mathbf{S}$ consists of a purely volumetric contribution and a purely isochoric one. Moreover, one obtains the following noticeable relations $\partial_{\mathbf{C}} J = \frac{1}{2} J\mathbf{C}^{-1}$ and $\mathsf{P} = \partial_{\mathbf{C}}\bar{\mathbf{C}} = J^{-2/3}[\mathsf{I} - \frac{1}{3}\mathbf{C} \otimes \mathbf{C}^{-1}]$. P is the fourth-order projection tensor and I denotes the fourth-order unit tensor, which, in index notation, has the form $\mathsf{I}_{IJKL} = \frac{1}{2}[\delta_{IK}\delta_{JL} + \delta_{IL}\delta_{JK}]$. The projection tensor P furnishes the physically correct deviatoric operator in the Lagrangian description, i.e. $DEV[\cdot] = (\cdot) - 1/3\big(\bar{\mathbf{C}} : (\cdot)\big)\bar{\mathbf{C}}^{-1}$.

Note that it is possible to obtain the Cauchy stress tensor by applying the push-forward operation to (7) $\sigma = J^{-1}\chi_*(\mathbf{S})$ [37]. Hence:

$$\sigma = \sigma_{\text{vol}} + \bar{\sigma} = p\mathbf{1} + \frac{1}{J} dev\left[\bar{\mathbf{F}}\tilde{\mathbf{S}}\bar{\mathbf{F}}^{\mathbf{T}}\right] = p\mathbf{1} + \frac{1}{J} dev[\tilde{\sigma}] = p\mathbf{1} + {}_{\mathsf{P}} : \tilde{\sigma}, \tag{8}$$

where we have introduced the projection tensor ${}_{\mathsf{P}} = J^{-1}[\mathsf{I} - \frac{1}{3}\mathbf{1} \otimes \mathbf{1}]$ which furnishes the physically correct deviatoric operator in the Eulerian description, i.e. $dev[\cdot] = (\cdot) - \frac{1}{3} tr[\cdot]\mathbf{1}$.

Based on the kinematic decomposition of the deformation gradient tensor, the tangent operator, also known as the elasticity tensor when dealing with elastic constitutive laws, is defined in the reference configuration as

$$\begin{aligned}\mathsf{C} = 2\frac{\partial \mathbf{S}(\mathbf{C}, \mathbf{M}, \mathbf{N})}{\partial \mathbf{C}} &= \mathsf{C}_{\text{vol}} + \bar{\mathsf{C}} = 2\frac{\partial \mathbf{S}_{\text{vol}}}{\partial \mathbf{C}} + 2\frac{\partial \bar{\mathbf{S}}}{\partial \mathbf{C}} \\ &= 4\left[\frac{\partial^2 \Psi_{\text{vol}}(J)}{\partial \mathbf{C} \otimes \partial \mathbf{C}} + \frac{\partial^2 \bar{\Psi}(\bar{\mathbf{C}}, \mathbf{M}, \mathbf{N})}{\partial \mathbf{C} \otimes \partial \mathbf{C}}\right],\end{aligned} \tag{9}$$

where

$$\mathsf{C}_{\text{vol}} = 2\mathbf{C}^{-1} \otimes \left(p\frac{\partial J}{\partial \mathbf{C}} + J\frac{\partial p}{\partial \mathbf{C}} + 2Jp\frac{\partial \mathbf{C}^{-1}}{\partial \mathbf{C}}\right) = J\tilde{p}\mathbf{C}^{-1} \otimes \mathbf{C}^{-1} - 2J\mathsf{I}_{C^{-1}}, \tag{10}$$

with $(\mathsf{I}_{C^{-1}})_{IJKL} = -\left(\mathbf{C}^{-1} \odot \mathbf{C}^{-1}\right)_{IJKL} = -\frac{1}{2}\left(C^{-1}_{IK}C^{-1}_{JL} + C^{-1}_{IL}C^{-1}_{JK}\right)$, and $\tilde{p} = p + J\frac{dp}{dJ}$. The term $\bar{\mathsf{C}}$ corresponding to the deviatoric part is given by:

$$\bar{\mathsf{C}} = -\frac{4}{3}J^{-\frac{4}{3}}\left(\frac{\partial\bar{\Psi}}{\partial\bar{\mathbf{C}}}\otimes\bar{\mathbf{C}}^{-1} + \bar{\mathbf{C}}^{-1}\otimes\frac{\partial\bar{\Psi}}{\partial\bar{\mathbf{C}}}\right) + \frac{4}{3}J^{-\frac{4}{3}}\left(\frac{\partial\bar{\Psi}}{\partial\bar{\mathbf{C}}} : \bar{\mathbf{C}}\right) \times \left(\mathbb{I}_{\bar{C}^{-1}} - \frac{1}{3}\bar{\mathbf{C}}^{-1}\otimes\bar{\mathbf{C}}^{-1}\right) + J^{-\frac{4}{3}}\bar{\mathsf{C}}_{\bar{w}}, \tag{11}$$

where term $\bar{\mathsf{C}}_{\bar{w}}$ is defined as:

$$\bar{\mathsf{C}}_{\bar{w}} = 4\frac{\partial^2\bar{\Psi}}{\partial\bar{\mathbf{C}}\partial\bar{\mathbf{C}}} - \frac{4}{3}\left[\left(\frac{\partial^2\bar{\Psi}}{\partial\bar{\mathbf{C}}\partial\bar{\mathbf{C}}} : \bar{\mathbf{C}}\right)\otimes\bar{\mathbf{C}}^{-1} + \bar{\mathbf{C}}^{-1}\otimes\left(\frac{\partial^2\bar{\Psi}}{\partial\bar{\mathbf{C}}\partial\bar{\mathbf{C}}} : \bar{\mathbf{C}}\right)\right] + \frac{4}{9}\left(\bar{\mathbf{C}} : \frac{\partial^2\bar{\Psi}}{\partial\bar{\mathbf{C}}\partial\bar{\mathbf{C}}} : \bar{\mathbf{C}}\right)\bar{\mathbf{C}}^{-1}\otimes\bar{\mathbf{C}}^{-1}. \tag{12}$$

Note that its spatial counterpart of (9) is obtained from the application of the push-forward operation to (9) $\mathsf{c} = J^{-1}\boldsymbol{\chi}_*(\mathsf{C})$ [8]. Hence:

$$\mathsf{c} = \mathsf{c}_{\text{vol}} + \bar{\mathsf{c}}, \tag{13}$$

where:

$$\mathsf{c}_{\text{vol}} = (\tilde{p}\mathbf{1}\otimes\mathbf{1} - 2p\mathsf{I}). \tag{14}$$

The deviatoric term, $\bar{\mathsf{c}}$, can be obtained using the expression

$$\bar{\mathsf{c}} = \frac{2}{3}tr(\bar{\sigma})_{\mathsf{P}} - \frac{2}{3}(\mathbf{1}\otimes dev(\bar{\sigma}) + dev(\bar{\sigma})\otimes\mathbf{1}) + \bar{\mathsf{c}}_{\bar{w}}, \tag{15}$$

where $\bar{\mathsf{c}}_{\bar{w}}$ in (15) is the weighted push forward of $\bar{\mathsf{C}}_{\bar{w}}$

$$\bar{\mathsf{c}}_{\bar{w}} = {}_{\mathsf{P}}\!:\bar{\mathsf{C}}:_{\mathsf{P}}. \tag{16}$$

For a more detailed derivation of the material and spatial elasticity tensors for fully incompressible or compressible fibered hyperelastic materials and their explicit expressions, see i.e. [26] or [42].

The assumption that the anisotropic terms only contribute to the global mechanical response of the tissue when fibers are stretched, that is, $\bar{I}_i > \bar{I}_{i_0}$ is related to the waving of the collagen fibers [39] and represents a very simple framework to consider this waving. However, from a continuum mechanics point of view, a more elegant formulation to consider the waving is the dual mechanism constitutive theory initially proposed for polymeric and elastomeric materials by Tobolsky et al. [57] and Wineman and Rajagopal [60], respectively, and for biological tissues by Wulandana and Robertson [61]. The first mechanism is associated to the matrix

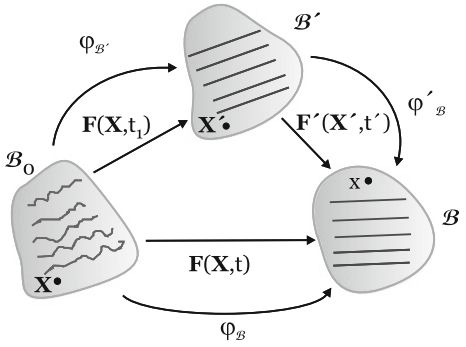

Fig. 2 Schematic of relevant reference configurations for the dual mechanism constitutive model [40]

tissue and the second mechanism, associated to the fibers, has a different unloaded configuration, corresponding to non-zero loading of the original material.

A brief discussion of the kinematics necessary for the dual mechanism constitutive equation is given below. A schematic of relevant reference configurations is given in Fig. 2. The section of fibred tissue will be represented by a three-dimensional body B which initially, say at time $t = t_0$, is stress free and occupies a region that will be referred to as the undeformed reference configuration $\mathscr{B}_0$. We consider a typical material particle, $\mathbf{X} \in \mathscr{B}_0$, in the body B. Using this notation, the motion of an arbitrary material particle can be described through the relationship $\mathbf{x} = \boldsymbol{\varphi}_{\mathscr{B}}(\mathbf{X}, t)$. The deformation gradient $\mathbf{F}$ at time t for an arbitrary material particle relative to the reference configuration $\mathscr{B}_0$ is given by $\mathbf{F}(\mathbf{X}, t) = \mathbf{F}_{\mathscr{B}}(\mathbf{X}, t) := \frac{\partial \boldsymbol{\varphi}_{\mathscr{B}}(\mathbf{X},t)}{\partial \mathbf{X}}$. The mechanical response of the first mechanism (matrix) will only be a function of $\mathbf{F}$. At some critical level of deformation, the second mechanism (fibers) is presumed to commence load bearing. The contribution of the second mechanism to load bearing is presumed to be a function of the deformation relative to $\mathscr{B}'$. Let $\mathbf{X}'$ denote the coordinates of the particle that was in position $\mathbf{X}$ in $\mathscr{B}_0$. If the configuration $\mathscr{B}'$ is reached at some time $t = t_1$, then $\mathbf{X}' = \boldsymbol{\varphi}_{\mathscr{B}'}(\mathbf{X}, t_1)$. The motion of an arbitrary material particle may then be described relative to the $\mathscr{B}_0$ configuration in standard form or $\mathscr{B}'$ as $\mathbf{x} = \boldsymbol{\varphi}'_{\mathscr{B}}(\mathbf{X}', t')$ with $t' = t - t_1$. The deformation gradient $\mathbf{F}'$, relative to the reference configuration $\mathscr{B}'$ is given by $\mathbf{F}'(\mathbf{X}', t') = \mathbf{F}'_{\mathscr{B}}(\mathbf{X}_1, t') := \frac{\partial \boldsymbol{\varphi}'_{\mathscr{B}'}(\mathbf{X}',t')}{\partial \mathbf{X}'}$. After operations, we obtain that $\mathbf{F}'(\mathbf{X}', t') = \mathbf{F}_{\mathscr{B}}(\mathbf{X}, t) \cdot \mathbf{F}^{-1}_{\mathscr{B}}(\mathbf{X}, t_1)$. The fiber activation occurs (second mechanism) when $\lambda_i = \lambda_{i_0}$ and both mechanisms will be active as load bearing components.

By particularization of this framework to fibred soft biological tissues, we have that the matrix is associated to the first mechanics and collagen fibers with the second and deform with $\mathbf{F}(\mathbf{X}, t)$ and $\mathbf{F}'(\mathbf{X}', t')$ respectively. In this context, the SEF presented in (4) is

$$\begin{aligned}\overline{\Psi}\left(\bar{\mathbf{C}}(\mathbf{X},t),\mathbf{M},\mathbf{N}\right) &= \overline{\Psi}_{\text{iso}}\left(\bar{\mathbf{C}}(\mathbf{X},t)\right) + \overline{\Psi}_{\text{ani}}\left(\bar{\mathbf{C}}'(\mathbf{X}',t'),\mathbf{M},\mathbf{N}\right)\\ &= \mu_1[\bar{I}_1(\mathbf{X},t)-3] + \mu_2[\bar{I}_2(\mathbf{X},t)-3]\\ &\quad + \frac{\gamma}{a\eta}\left[\exp\left(\eta[\bar{I}_1(\mathbf{X},t)-3]^a\right) - f(\bar{I}_1(\mathbf{X},t),a)\right]\\ &\quad + \sum_{i=4,6}\frac{c_{i-3}}{bc_{i-2}}\left[\exp\left(c_{i-2}[\bar{I}_i(\mathbf{X}',t')-1]^b\right) - g(\bar{I}_i(\mathbf{X}',t'),b)\right],\end{aligned} \tag{17}$$

where $\bar{I}_i(\mathbf{X}',t') = \bar{\lambda}_i^2(\mathbf{X}',t')$ and $\bar{\lambda}_i(\mathbf{X}',t') = \bar{\lambda}_i(\mathbf{X},t)/\bar{\lambda}_i(\mathbf{X},t_1) = \lambda_i(\mathbf{X},t)/\bar{\lambda}_{i_0}$. Finally, $\bar{\lambda}_{i_0} \geq 1$ is regarded as the initial crimping of the fibers. From the next and for simplicity of the nomenclature, we denote $\bar{I}_i(\mathbf{X},t) = \bar{I}_i$ and $\bar{I}_i(\mathbf{X}',\ t') = \bar{I}_{i'}$, so $\bar{\lambda}_{i'} = \bar{\lambda}_i/\bar{\lambda}_{i_0}$ and

$$\begin{aligned}\bar{\Psi}\ (\bar{\mathbf{C}}_1,\ \mathbf{M},\ \mathbf{N}) &= \mu_1[\bar{I}_1-3] + \mu_2[\bar{I}_2-3] + \frac{\gamma}{a\eta}\left[\exp\left(\eta[\bar{I}_1-3]^a\right) - f(\bar{I}_1,a)\right]\\ &\quad + \sum_{i=4,6}\frac{c_{i-3}}{bc_{i-2}}\left[\exp\left(c_{i-2}[\bar{I}_i'-1]^b\right) - g(\bar{I}_i',b)\right].\end{aligned} \tag{18}$$

3 Micro-Structurally Based Models: Elastic Behavior

The models proposed for soft tissues could be classified into two groups. The first comprises the macroscopic models previously presented, in which a SEF is obtained disregarding the nature of the micro-structural components of the tissue. Second, a group of micro-structurally based models are presented in this section, in which the macroscopic mechanical properties are obtained by assuming a constitutive relation for the microscopic components along each direction, whereas the macroscopic behaviour is obtained by integration of the contributions in all directions of space.

Gasser et al. [23] proposed the SEF

$$\bar{\Psi}(\mathbf{C},\mathbf{M},\mathbf{N}) = \mu[\bar{I}_1-3] + \frac{k_1}{2k_2}[\exp(k_2[\kappa\bar{I}_1 + [1-3\kappa]\bar{I}_4 - 1]^2) - 1] \tag{19}$$

$$+\frac{k_3}{2k_4}[\exp(k_4[\kappa\bar{I}_1 + [1-3\kappa]\bar{I}_6 - 1]^2) - 1], \tag{20}$$

where $\kappa \in [0, 1/3]$ is a measure of the dispersion of the fibers around the preferred orientations. This parameter is a result of considering the fibers oriented following the von Mises orientation density function. Thus, $\kappa = 1/3$ means isotropy and $\kappa = 0$ no fiber dispersion.

Anisotropy can straightforwardly introduced in micro-structurally based models by considering an orientation density function, ρ, weighting the contribution of the fibers in space

$$\bar{\Psi} = \frac{3}{4\pi} \int_{\mathbb{U}^2} \rho \bar{\Psi} \mathrm{d}A. \tag{21}$$

First contributions considering this approach are due to Lanir [33], who proposed a structural model for planar tissues assuming that fibers are arranged in three-dimensional but almost planar wavy array. Thus, collagen fibers were restricted to a plane in which they were oriented following a Gaussian distribution around a mean preferred direction. The same assumption was adopted for the elastin fibers, which were oriented following a different distribution.

More recently, Alastrue et al. [1] proposed a hyperelastic microsphere-based model with statistically distributed fibers. In that model, it is assumed the existence of a uniaxial orientation distribution function $\rho(\mathbf{r};\mathbf{a}) = \rho(-\mathbf{r};\mathbf{a})$ for $\mathbf{r} \in \mathbb{U}^2$ a referential unit vector and $\mathbb{U}^2$ the unit sphere surface. The macroscopic strain energy density corresponding to one family of fibers associated with the so-called preferred direction $\mathbf{a}$ and with n fibers per unit volume is then defined as

$$\bar{\Psi}_{\mathrm{f}} = \sum_{i=1}^{n} \rho(\mathbf{r}^i;\mathbf{a}) \bar{\Psi}_{\mathrm{f}}^i, \tag{22}$$

where $\mathbf{r}^i$ are referential unit vectors associated with the direction of the ith fiber, and Ψ_{f}^i is the fiber's strain energy according to the deformation in the direction of $\mathbf{r}^i$. When expanding this expression in order to account for N preferred orientations $\mathbf{a}_I$ related to different families of fibers one obtains

$$\bar{\Psi}_{\mathrm{ani}} = \sum_{I=1}^{N} \bar{\Psi}_{\mathrm{f}}^I = \sum_{I=1}^{N} \langle n\rho_I \bar{\Psi}_{\mathrm{f}}(\bar{\lambda}) \rangle = \frac{1}{4\pi} \int_{\mathbb{U}^2} n\rho_I \bar{\Psi}_{\mathrm{f}} \mathrm{d}A. \tag{23}$$

Apart from the symmetry condition $\rho(\mathbf{r};\mathbf{a}) = \rho(-\mathbf{r};\mathbf{a})$ it was considered that fibers are rotationally symmetrically distributed with respect to the preferred mean orientation $\mathbf{a}$—in other words, $\rho(\mathbf{Q}\cdot\mathbf{r};\mathbf{a}) = \rho(\mathbf{r};\mathbf{a})\ \forall\ \mathbf{Q} \in \mathbb{Q}_+^3$ with rotation axis $\mathbf{a}$. As a consequence of the uniaxial distribution assumed for the one family of fibers considered, ρ can be defined as a function of the so-called mismatch angle $\omega = \arccos(\mathbf{a}\cdot\mathbf{r})$.

In Alastrue et al. [1], it was adopted the frequently applied π-periodic von Mises orientation distribution function (ODF)

$$\rho(\theta) = 4\sqrt{\frac{b}{2\pi}}\frac{\exp(b[\cos(2\theta)+1])}{\mathrm{erfi}(\sqrt{2b})}, \tag{24}$$

where the positive concentration parameter b constitutes a measure of the degree of anisotropy. Moreover, $\mathrm{erfi}(x) = -i\mathrm{erf}(x)$ denotes the imaginary error function with $\mathrm{erf}(x)$ given by

$$\mathrm{erf}(x) = \sqrt{\frac{2}{\pi}}\int_0^x \exp(-\xi^2)\mathrm{d}\xi. \tag{25}$$

Recently, the ODF Bingham [7] was proposed by Alastrue et al. [5] to account for the dispersion of the collagen fibrils with respect to their preferential orientation. That function is expressed as

$$\rho(r;A)\frac{\mathrm{d}A}{4\pi} = [K(A)]^{-1}\exp(r^{\mathrm{t}}\cdot A\cdot r)\frac{\mathrm{d}A}{4\pi}, \tag{26}$$

where A is a symmetric 3×3 matrix, $\mathrm{d}A$ is the Lebesgue invariant measure on the unit sphere, $r\in\mathbb{U}^2$ and $K(A)$ is a normalizing constant. As its main features, it is worth noting that this distribution always exhibits antipodal symmetry, but not rotational symmetry for the general case.

Applying straightforward transformations, Eq. (26) can be rewritten as

$$\rho(r;Z,Q)\frac{\mathrm{d}A}{4\pi} = [F_{000}(Z)]^{-1}\mathrm{etr}(Z\cdot Q^{\mathrm{t}}\cdot r\cdot r^{\mathrm{t}}\cdot\ Q)\frac{\mathrm{d}A}{4\pi}, \tag{27}$$

where $\mathrm{etr}(\cdot)\equiv\exp(\mathrm{tr}(\cdot))$, Z is a diagonal matrix with eigenvalues $\kappa_{1,2,3}$, $Q\in\mathbb{Q}^3$ such that $A = Q\cdot Z\cdot Q^{\mathrm{T}}$ and $F_{000}(Z)$ may be written as

$$F_{000}(Z) = [4\pi]^{-1}\int_{\mathbb{U}^2}\mathrm{etr}(Z\cdot r\cdot r^{\mathrm{t}})\mathrm{d}A = {}_1F_1(\frac{1}{2};\frac{3}{2};Z), \tag{28}$$

with ${}_1F_1$ a confluent hypergeometric function of matrix argument as defined by Herz [25].

Thus, the probability concentration is controlled by the eigenvalues of Z, which might be interpreted as concentration parameters. Specifically, the difference between pairs of $\kappa_{1,2,3}$—i.e., $[\kappa_1-\kappa_2]$, $[\kappa_1-\kappa_3]$ and $[\kappa_2-\kappa_3]$—determines the shape of the distribution over the surface of the unit sphere, Fig. 3. Therefore, the value of one of these three parameters may be fixed to a constant value without reducing the versatility of (27). In fact, setting two of the parameters equal to zero the Von Mises ODF is obtained and when two parameters come close up, a rotational symmetry is achieved.

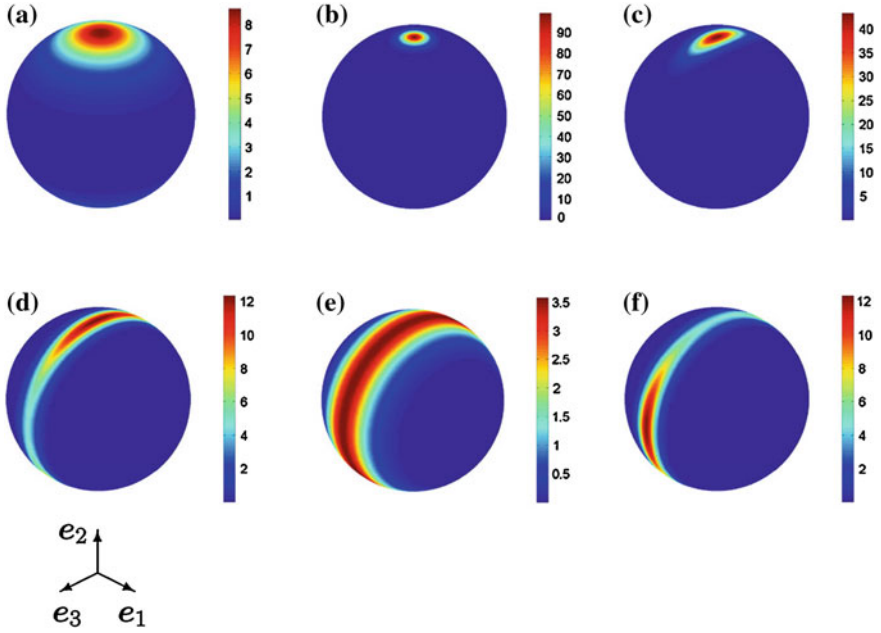

Fig. 3 Representation of the Bingham ODF for different sets of parameters with $\kappa_1 = 0.0$ [5]. **a** $\kappa_2 = 0.0, \kappa_3 = 5.0$. **b** $\kappa_2 = 0.0, \kappa_3 = 50.0$. **c** $\kappa_2 = 40.0, \kappa_3 = 50.0$. **d** $\kappa_2 = 49.0, \kappa_3 = 50.0$. **e** $\kappa_2 = 10.0, \kappa_3 = 10.0$. **f** $\kappa_2 = 50.0, \kappa_3 = 49.0$

Measurements of 3D organization of the collagen fibers, which are birefringent, can be made with the universal stage, an attachment to the polarizing microscope. The calibrated rotational movement, in three dimensions, of the inner stage of the universal stage permits the measurement of directional alignment of individual fibers, relative to the reference plane of the section [11, 12, 15, 53]. The experimental data obtained by Garcia [18] was fitted using the ODF Bingham, Table 1.

Once the ODF is fitted by means of microstructural observations [18, 22], it is necessary to fit the rest of the material constitutive parameters. For the isotropic component of elastin, we use two different SEF for $\bar{\Psi}_{\text{iso}}$, the classical Neo-Hookean model

$$\bar{\Psi}_{\text{iso}} = \mu[\bar{I}_1 - 3], \tag{29}$$

and the Demiray's SEF [13]

$$\bar{\Psi}_{\text{iso}} = \frac{c_1}{c_2}\left[\exp\left(\frac{c_2}{2}[\bar{I}_1 - 3]\right) - 1\right]. \tag{30}$$

Table 1 Bingham distribution parameters that determine the collagen orientation density in the porcine wall [18]

	Family 1			Family 2		
	κ_1	κ_2	κ_3	κ_1	κ_2	κ_3
All proximal	9.6	0.0	22.4	18.6	0.0	30.3
All distal	18.6	0.0	30.6	15.5	0.0	28.4

Finally, phenomenological strain energy density function proposed by Holzapfel et al. [26] was used to approach the fiber response

$$n\bar{\psi}_f^i(\bar{\lambda}_i) = \frac{k_1}{2k_2}\left(e^{k_2((\bar{\lambda}_i)^2-1)^2} - 1\right) \qquad if \qquad \bar{\lambda}_i \geq 1 \tag{31}$$

where $\bar{\lambda}_i = \left\|\bar{\mathbf{t}}^i\right\|$ defines the isochoric stretch in the fiber direction $\mathbf{r}^i$ and assuming $n\bar{\psi}_f^i(\bar{\lambda}_i) = 0$ when $\left(\bar{\lambda}_i\right) < 1$, since it is known that collagen fibers only affects to the global mechanical behavior in tensile states. Basically the parameters μ or c_1 and c_2 corresponding to the mechanical behavior of the isotropic part (Neo-Hookean or Demiray's SEF) and k_1 and k_2 for anisotropic one.

Due to lack of experimental data of the specimens analyzed in this work, experimental uniaxial tension tests previously developed in our group for porcine carotids in a proximal and distal regions were fitted [20]. The fitting of the experimental mechanical data was developed by using a Levenberg-Marquardt type minimization algorithm [36], by defining the objective function considering an isochoric tissue, Eq. (32). In this function, $\sigma_{\theta\theta}$ and σ_{zz} are the Cauchy (true) stress data obtained from the tests, $\sigma_{\theta\theta}^{\bar{\Psi}}$ and $\sigma_{zz}^{\bar{\Psi}}$ are the Cauchy stresses for the ith point computed following Eq. (33), and n is the number of data points.

$$\chi^2 = \sum_{i=1}^{n}\left[\left(\sigma_{\theta\theta} - \sigma_{\theta\theta}^{\Psi}\right)_i^2 + \left(\sigma_{zz} - \sigma_{zz}^{\Psi}\right)_i^2\right], \tag{32}$$

where

$$\sigma_{\theta\theta}^{\Psi} = \lambda_\theta \frac{\partial \Psi}{\partial \lambda_\theta} \quad \sigma_{zz}^{\Psi} = \lambda_z \frac{\partial \Psi}{\partial \lambda_z}. \tag{33}$$

The goodness of the fitting was measured by computing the coefficient of determination of the normalized mean square root error ε was computed for each fitting $\varepsilon = \frac{\sqrt{\frac{\chi^2}{n-q}}}{\mu}$. In this equation μ the mean value of the measured stresses $\mu = \frac{\sum_{i=1}^{n}(\sigma)_i}{n}$, q is the number of parameters of the SEF, so $n - q$ is the number of degrees of freedom, and μ the mean stress already defined above.

Figure 4 illustrates the results of the mean of the proximal and distal specimens which was fitted based on the isotropic Neo-Hookean or Demiray SEFs. In this

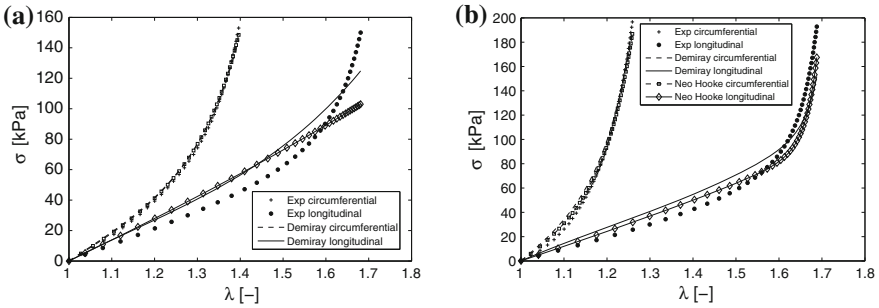

Fig. 4 Stress-stretch curves fitting [18] of the uniaxial tension tests from [20]. **a** Proximal specimens. **b** Distal specimens

Table 2 Structural material coefficients for the both SEF considered [18]

Neo-Hookean SEF	Specimen	μ (kPa)	k_1 (kPa)	$k_2(-)$	ε	
	Proximal	46	5.1	1.42	0.145	
	Distal	40	20	3.2	0.1574	
Demiray' SEF	Specimen	c_1 (kPa)	$c_2(-)$	k_1 (kPa)	k_2 (−)	ε
	Proximal	7.640	1.250	5.910	1.955	0.095
	Distal	14.98	0.830	21.04	2.995	0.124

case, the Neo-Hookean model resulted in an excellent fit for the distal specimen, showing a $\varepsilon = 0.110$. However, it substantially underestimated the proximal results in the longitudinal curve with a $\varepsilon = 0.145$. This shows that although the linear model of the isotropic part can very well describe the distal, it falls when proximal data is considered. The nonlinear model for the isotropic part improve the numerical fitting. It can be seen that the proposed nonlinear model can describe both proximal and distal data. The fit based on the Demiray SEF for elastin gave smaller normalized mean square root error ($\varepsilon = 0.124$ and $\varepsilon = 0.095$). The material coefficients corresponding to the fitting results are shown in the Table 2.

4 Micro-structurally Based Models: Softening and Damage Behavior

4.1 Probabilistic Damage Model

Histological studies performed in a number of soft tissues [14, 30] have shown that elastic fibers appear to be wavy and distributed about preferential directions [34]. Thus, as the load is applied, more and more fibers start to bear load. However, the degree of straightening of each fiber will also depend upon its orientation relative to

the loading and the interstitial matter which might avoid its complete straightening. A model that consider the wavy nature of elastic fibers was proposed by Rodriguez et al. [45, 46]. Each bundle of fibers is assumed to behave following the worm-like eight-chain model proposed by Arruda and Boyce [6]

$$n\bar{\Psi}_{\mathrm{f}}(\bar{\lambda}) = \begin{cases} 0 & \text{if} \quad \bar{\lambda} < 1 \\ B[2\frac{\bar{r}^2}{L^2} + \frac{1}{1-\bar{r}/L} - \frac{\bar{r}}{L} & \\ -\frac{\ln(\bar{\lambda}^4 r_0^2)}{4r_0 L}[4\frac{r_0}{L} + \frac{1}{[1-r_0/L]^2} - 1] - \Psi_{\mathrm{r}}] & \text{if} \quad \bar{\lambda} \leq 1 \end{cases}, \tag{34}$$

with $B = \frac{1}{4}nK\Theta r_0/A$ a stress-like material parameter, L the maximum fiber length, r_0 the fiber length in the undeformed configuration, $\bar{r} = \bar{\lambda} r_0 < L$ the actual fiber length, $\bar{\lambda}$ the actual isochoric fiber stretch, and

$$\Psi_{\mathrm{r}} = 2\frac{r_0^2}{L^2} + \frac{1}{1 - r_0/L} - \frac{r_0}{L}, \tag{35}$$

being a repository constant accounting for a zero strain energy at $\bar{\lambda} = 1$. This model considers the maximum fiber length, L, as a Beta random variable, and assumes the same average orientation for all fibers within the bundle as well as that fibers do not bear compressive loads. Hence, the strain energy density function for a bundle of fibers is given by

$$\bar{\Psi}_{\mathrm{bun}}(\bar{\lambda}, \bar{\lambda}_{t^*}) = \begin{cases} 0, & \bar{\lambda} < 1, \\ \int_1^{\bar{\lambda}} \int_{a(r_0\bar{\lambda}_{t^*})}^{\iota} \bar{\Psi}'_{\mathrm{f}}(\xi, x)\ell_L(x)\mathrm{d}x\mathrm{d}\xi, & \bar{\lambda} \geq 1, \end{cases} \tag{36}$$

where $a(r_0\bar{\lambda}_{t^*})$ is a monotonically increasing function that determines the minimal fiber length within the bundle for which failure has not yet occurred,[1] $\Psi'_{\mathrm{f}} = n\partial\Psi_{\mathrm{f}}/\partial\bar{\lambda}$, and $\ell_L(x)$ is a Beta probability density function with parameters γ and η

$$\ell_L(x) = \frac{1}{\iota - r_0}\frac{\Gamma(\eta + \gamma)}{\Gamma(\eta)\Gamma(\gamma)}\left[\frac{x - r_0}{\iota - r_0}\right]^{\gamma - 1}\left[1 - \frac{x - r_0}{\iota - r_0}\right]^{\eta - 1}, \quad x \in [r_0, \iota]. \tag{37}$$

The parameter $\bar{\lambda}_{t^*}$ in (36) corresponds to the maximum isochoric fiber stretch attained by the bundle over the past history up to time $t \in \mathscr{T}_+$. Therefore, the damage of the fiber bundle increases whenever $\bar{\lambda}_t - \bar{\lambda}_{t^*} \geq 0$ and, therefore, it is strain driven. On the other hand, function $a(r_0\bar{\lambda}_{t^*})$ determines the minimum fiber length within the bundle for which failure has not yet occurred, and is given by

[1] Notice that x is a dummy variable used for integration purposes.

$$a(r_0\bar{\lambda}_{t^*}) = \exp\left(\left[\frac{r_0\bar{\lambda}_{t^*}}{\delta}\right]^{\varpi}\right) r_0\bar{\lambda}_{t^*}, \tag{38}$$

where ϖ and δ are dimensionless model parameters. Note that with this form of $a(r_0\bar{\lambda}_{t^*})$, the bundle will degrade faster as the deformation gets larger (i.e., longer fiber will fail at a smaller fraction of their maximum length).

With these considerations at hand, fiber damage is quantified as

$$\begin{aligned} D_{\mathrm{f}} &= \frac{1}{\imath - r_0}\frac{\Gamma(\eta+\gamma)}{\Gamma(\eta)+\Gamma(\gamma)} \int_{r_0}^{a\left(r_0\bar{\lambda}_t\right)} \left[\frac{x-r_0}{\imath-r_0}\right]^{\gamma-1}\left[1-\frac{x-r_0}{\imath-r_0}\right]^{\eta-1} \mathrm{d}x \\ &= \mathrm{Beta}\left(\frac{a(r_0\bar{\lambda}_t)}{\imath-r_0}, \gamma, \eta\right). \end{aligned} \tag{39}$$

Rodriguez et al. [45] used the damage model to study the balloon inflation of a coronary artery 40 mm long, with an inner diameter of 2.7 mm and a thickness of 1.8 mm. The artery has been simulated as a multi-layer composite material by considering the media, and adventitia layers and included the residual stresses. Figure 5 shows the damage distributions in the arterial wall under balloon inflation. The balloon induces large longitudinal and circumferential stretching in the artery which causes larger fiber deformation in the adventitia than in the media leading to larger stresses and more rapid damage of this layer.

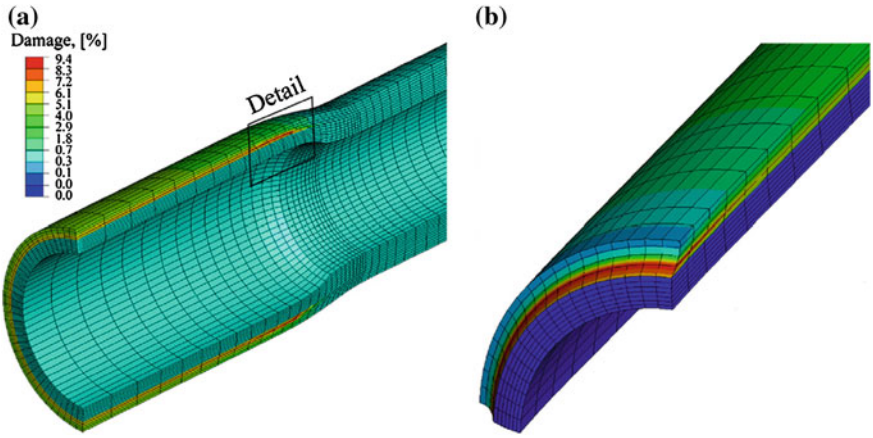

Fig. 5 Damage distribution in the arterial wall under balloon inflation from [45]

4.2 Deterministic Damage Model

If an uniaxial tension is developed six distinct stages A-H should be considered, Fig. 6—for clarity only one family of fibers is considered when furnished with matrix (light grey background) and fibers (wavy dark solid lines)—. Stage A is defined by $\lambda = 1$. After that, stage B, the uniaxial loading is small and the collagen fibers to become less wavy without contributing significantly to load bearing—only first mechanism—$(\lambda < \lambda_o)$. When $\lambda \geq \lambda_o$, the tissue has been loaded just to the level where the fibers have straightened and will resist further extension—both mechanism are bearing load (stage C). If the strip of fibred tissue is unloaded, the fibers had not returned to the original unstrained wave pattern but remained in a straightened state—this fact means that the reference configuration for the second mechanism has changed $\left(\lambda_o^*\right)$—a softened behavior until free-stress state (stage D)—. Subsequent reloading follows the former unloading curve until the previous maximum stretch is reached. However, during stage E the fibers are less wavy, so critical level of deformation for the second mechanism to start load bearing has also change and this stage D is characterized by $\lambda < \lambda_o^*$. When $\lambda \geq \lambda_o^*$ fibers again resist further extension, however if loading level $\lambda_{\min}$ is reached some fibers are disrupted, stage G, with partial collagen disruption. Upon further loading, only some fibers will resist stretch until $\lambda = \lambda_{\max}$ where bond rupture and complete damage is produced (stage H).

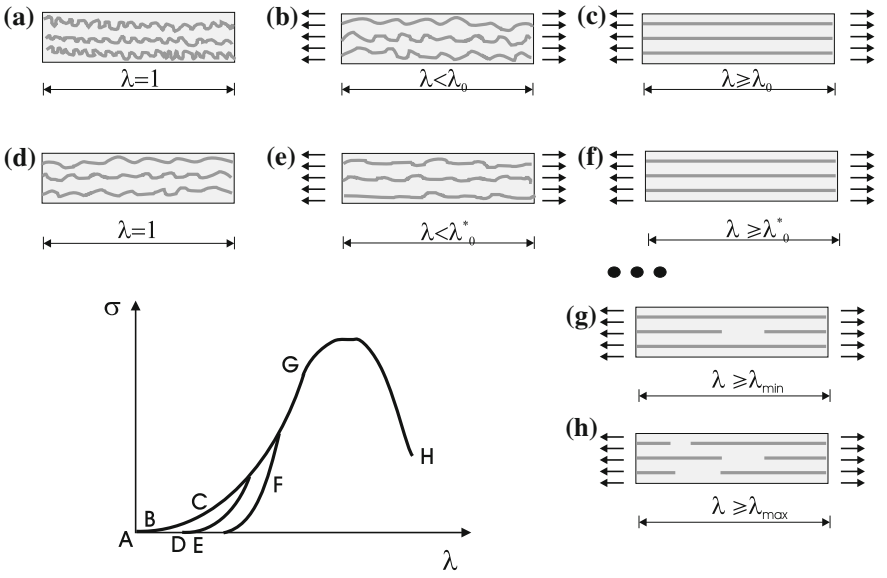

Fig. 6 Schematic representation of stages of tissue deformation. **a** Initial unloaded tissue. **b** Only matrix load bearing $\left(I_{io} = \lambda_o^2\right)$. **c** Fibers load bearing. **d** Initial state after unloading. **e** Only matrix load bearing after unloading $\left(w_i \lambda_i = \lambda_o^*\right)$. **f** Fibers load bearing after unloading. **g** Partial disruption of fibers. **h** Total disruption of the fibers, [40]

The experimental results suggest that just like the elastic properties, the inelastic behavior of soft tissues is also characterized by anisotropy [3, 41, 43, 44]. Accordingly, a suitable constitutive model should account for this directional dependence and take into account the different alteration mechanisms associated with this anisotropy. The phenomenological inelastic model should include the Mullins effect, the permanent set resulting from the residual strains after unloading, and the fibre and matrix disruption associated to supraphysiological loads or strains [9].

To model these inelastic processes, we apply the following considerations:

- We have introduced the $\bar{\lambda}_{i_0}(i=4,6)$ parameter that governs the anisotropic contribution to the global mechanical response of the tissue only when stretched, that is, $\bar{\lambda}_i' = \bar{\lambda}_i/\bar{\lambda}_{i_0} \geq 1$. We modified this parameter by a weight factor w_i associated to $\bar{\lambda}_{i_0}$ that changes independently from each direction to take into account structural alterations along the fibers direction, that is, $\lambda_o^* = w_i \cdot \bar{\lambda}_{i_0}$. With this modification, we can reproduce at the same time the softening behavior and the permanent set presented in this kind of tissue.
- The preconditioning until "saturated" state is modelled using a continuous damage model that accumulates within the whole strain history of the deformation process by a weight factor $D_{r_k}(k=m,4,6)$ associated to the matrix ($\bar{I}_1$ and $\bar{I}_2$) and the fibers ($\bar{I}_i$) [44].
- Finally, the softening as a result of the bond rupture and complete damage is accomplished by using the classical Continuum Damage Mechanics (CDM) theory using the well-known reduction factors [50], $D_{s_k}(k=m,4,6)$, associated to the matrix ($\bar{I}_1$ and $\bar{I}_2$) and the fibers (I_i) [10].

With these considerations, the free energy for the fibers is assumed to be of the form

$$\begin{aligned}\bar{\Psi}_{\text{ani}}\langle n\rho\bar{\psi}_{\text{f}}(\lambda)\rangle &= [1-D]\frac{1}{4\pi}\int_{\mathbb{U}^2} n\rho\bar{\psi}_0(\bar{\lambda}^i)\mathrm{d}A \\ &\approx \sum_{j=1}^{N}\left[1-D_j\right]\left[\sum_{i=1}^{m} n\rho_i w^i \bar{\psi}_{j,0}^i(\bar{\lambda}^i)\right]\end{aligned} \tag{40}$$

with $D_j = D_j^\alpha + D_j^\beta$ the normalized scalars referred to as the damage, $D_j^\alpha : \mathbb{R}_+ \to \mathbb{R}_+$ and $D_j^\beta : \mathbb{R}_+ \to \mathbb{R}_+$ are monotonically increasing smooth functions with the following properties $D_j^\alpha(0)=0$, $D_j^\beta(0)=0$ and $D_j^\alpha + D_j^\beta \in [0,1]$ and $\bar{\psi}_0(\bar{\lambda}^j)$ the effective strain energy density functions of each j family of fibers.

The second law of thermodynamics asserts a non-negative rate of entropy production. Using standard arguments based on the Clausius-Duhem inequality [37]

$$\mathscr{D}_{int} = -\dot{\Psi} + \frac{1}{2}\mathbf{S} : \dot{\mathbf{C}} \geq 0 \tag{41}$$

yields

$$\mathscr{D}_{int} = -\sum_{j=1}^{N}\left[\frac{\partial\bar{\psi}_{j,0}}{\partial D_j^{\alpha}}\dot{D}_j^{\alpha} + \frac{\partial\bar{\psi}_{j,0}}{D_j^{\beta}}\dot{D}_j^{\beta} + \frac{\partial\bar{\psi}_{j,0}}{\partial w_j}\dot{w}_j\right] \geq 0 \tag{42}$$

where the thermodynamic forces are

$$\begin{aligned} f_j^{\alpha} &= -\frac{\partial\bar{\psi}_{j,0}(\bar{\lambda}^i)}{D_j^{\alpha}} = \bar{\psi}_{j,0}(\bar{\lambda}^i) \quad f_j^{\beta} = -\frac{\partial\bar{\psi}_{j,0}(\bar{\lambda}^i)}{D_j^{\beta}} = \bar{\psi}_{j,0}(\bar{\lambda}^i) \\ f_{w_j} &= -\frac{\partial\bar{\psi}_{j,0}(\bar{\lambda}^i)}{\partial w_j} = \partial\bar{\psi}_{j,0}(\bar{\lambda}^i) \end{aligned} \tag{43}$$

The thermodynamic forces f_{α}, f_{β} and f_{w_j} are conjugated to the internal variables D_j^{α}, D_j^{β} and w_j respectively.

4.2.1 Evolution of the Internal Variables

Continuous damage variables $\left(D_j^{\alpha}\right)$

The continuous damage D_j^{α} is assumed that accumulate within the whole strain history of the deformation process which is also governed by the local effective strain energy and have the form

$$D_j^{\alpha} = d_{\infty}^{j}\left[1 - \exp\left(-\frac{\alpha}{\zeta_j}\right)\right]$$

where

$$\alpha \doteq \int_0^t |\dot{f}_j(s)|ds \qquad \dot{r}_j = |\dot{f}_j| = \text{sign}(\dot{\Psi}_{j,0}^{0}) \tag{44}$$

with the initial condition $\alpha(0) = 0$. Finally, ζ_j is the damage saturation parameters and the parameters d_{∞}^{j} describe the maximum possible continuous damage, thus we have the constraint $d_{\infty}^{j} \in [0, 1]$ [44].

Discontinuous damage variables $\left(D_j^{\beta}\right)$

We define a damage criterion in the strain space by the condition that, at any time t of the loading process, the following expression is fulfilled [49]

$$\Phi_j(\overline{\lambda}(s), \Xi^*_{s,j}) = \Xi_j - \Xi^*_j = \sqrt{2\bar{\psi}_{j,0}(\overline{\lambda}^i(s))} - \Xi^*_j \leq 0, \tag{45}$$

where $\Xi^*_j = \max_{s\varepsilon(-\infty,t]}\left(\sqrt{2\bar{\psi}_{j,0}(\overline{\lambda}^i(s))}\right)$ signifies damage threshold (energy barrier) at current time t (i.e. the radius of the damage surface). If $\Phi_j < 0$, no damage occurs while $\Phi_j = 0$ defines the damage surface. Note that $\Phi_j > 0$ is an impossible situation. Update of this surface is needed when the free energy density of a material point or fiber goes up over Ξ^*_j

$$\Xi^*_j = \begin{cases} \dot{f}^\beta_j = \dot{\bar{\psi}}_{j,0}(\bar{\lambda}^i) & \text{if } \Phi_j = 0 \text{ and } \dot{f}^\beta_j > 0 \\ 0 & \text{otherwise} \end{cases} \tag{46}$$

The last equation needed for a complete definition of the model is the irreversible rate of the damage variable D^β_i

$$\frac{\mathrm{d}D^\beta_j}{\mathrm{d}t} = \begin{cases} h_j(\Xi_j)\dot{\Xi}_j & \text{if } \Phi_j = 0 \text{ and } \dot{f}^\beta_j > 0 \\ 0 & \text{otherwise} \end{cases} \tag{47}$$

where $h_j(\Xi_j) = \mathrm{d}D^\beta_j/\mathrm{d}\Xi_j$ are the functions that characterize the damage evolution in the material.

Following previous work [38], we consider the discontinuous damage evolution equation

$$D^\beta_j = \frac{1}{1 + \exp(-\varpi_j[\Xi_j - \gamma_j])}, \tag{48}$$

where the parameter ϖ_j controls the slope and γ_j defines the value Ξ such that $D^\beta_j = 0.5$.

Softening variables (w_j)

For the softening variables w_j, we consider the following criteria

$$\Upsilon_j(\mathbf{C}(t), \Gamma_{j_t}) = \frac{\partial \psi_{j,0}(\overline{\lambda}^i)}{\partial \overline{\lambda}^i} - \Gamma_{j_t} = \Gamma_j - \Gamma_{j_t} \leq 0 \tag{49}$$

where $\Gamma_j = \frac{\partial \psi_{j,0}(\overline{\lambda}^i)}{\partial \overline{\lambda}^i}$ is the softening stress release rate at time $t \in \mathbb{R}_+$ and Γ_{j_t} signifies the softening threshold (stress barrier) at current time t for matrix and fibers

$$\Gamma_{j_t} = \max_{sr\in(-\infty,t)} \frac{\partial \psi_{j,0}\left(\overline{\lambda}^i\right)}{\partial \overline{\lambda}^i} \tag{50}$$

The equation $\Upsilon_j(\mathbf{C}(t), \Gamma_{j_t}) = 0$ defines a softening surface in the strain space. With these means at hand, we finally propose the following set of rate equations for an evolution of the softening variables

$$\dot{w}_j \doteq \begin{cases} \kappa_j \dot{\Gamma}_{j_t} & \text{if} \quad \Upsilon = 0 \quad \text{and} \quad \mathbf{N}_j : \dot{\mathbf{C}} > 0 \\ 0 & \text{otherwise} \end{cases} \tag{51}$$

Let us now consider softening functions of the simple form

$$w_j = \kappa_j \Gamma_{j_t} + 1 \tag{52}$$

where κ_j is the only parameter to define the softening mechanism in each fiber direction.

4.2.2 Computational Aspects

If the material state is known at a time t_n and the deformation is known at a time $t_{n+1} = t_n + \Delta t$, we may write [32]

$$\mathbf{S}_{n+1} = J_{n+1} p_{n+1} \mathbf{C}_{n+1}^{-1} + J_{n+1}^{-\frac{2}{3}} \sum_{k=m,f_1,f_2} \left[1 - D_{j_{n+1}}\right] \bar{\mathbf{S}}^0_{(j)n+1}, \tag{53}$$

where the subscripts n and $n+1$ denote quantities evaluated at times t_n and t_{n+1}.

The iterative Newton procedure to solve a nonlinear finite element problem requires the determination of the consistent tangent material operator. This can be derived analytically for the given material Eq. (53). The symmetric algorithmic material tensor is expressed as [49, 51]

$$\begin{aligned} \mathsf{C}_{n+1} &= 2 \frac{\partial \mathbf{S}_{n+1}(\mathbf{C}_{n+1}, \mathbf{M}, \mathbf{N}, D_{(j)n+1}, w_{(j)n+1})}{\partial \mathbf{C}_{n+1}} = \mathsf{C}_{\mathrm{vol}_{n+1}} + \bar{\mathsf{C}}_{n+1} \\ &= 4 \left[\frac{\partial^2 \Psi_{\mathrm{vol}_{n+1}}(J_{n+1})}{\partial \mathbf{C}_{n+1} \otimes \partial \mathbf{C}_{n+1}} + \frac{\partial^2 \bar{\Psi}_{n+1}(\bar{\mathbf{C}}_{n+1}, \mathbf{M}, \mathbf{N}, D_{(j)n+1}, w_{(j)n+1})}{\partial \mathbf{C}_{n+1} \otimes \partial \mathbf{C}_{n+1}} \right] \\ &= \mathsf{C}_{\mathrm{vol}_{n+1}} + \sum_{j=m,f_1,f_2} \left[\left[1 - D_{(j)n+1}\right] \bar{\mathsf{C}}^0_{(j)n+1} - \bar{\mathsf{S}}_{(j)n+1} \right] \end{aligned} \tag{54}$$

where

$$\bar{\mathsf{S}}_{(j)n+1} = \begin{cases} \left[D'^{\alpha}_{(j)n+1} + D'^{\beta}_{(j)n+1} \operatorname{sign}(\dot{f}_{(j)n+1}) \right] \bar{\mathbf{S}}_{(j)n+1} \otimes \bar{\mathbf{S}}_{(j)n+1} - & \text{if} \quad \phi = 0 \\ -4 J^{-\frac{2}{3}} \frac{\kappa_j}{I_{j0}} \tilde{\Gamma}_j \frac{\partial^2 \bar{\Psi}_{n+1}}{\partial \Gamma_{jn+1}^2} \tilde{\mathbf{M}} \otimes \tilde{\mathbf{M}} & \text{and} \quad \mathbf{N}_{(j)n+1} : \dot{\mathbf{C}}_{n+1} > 0 \\ D'^{\beta}_{(j)n+1} \operatorname{sign}(\dot{f}_{(j)n+1}) \bar{\mathbf{S}}_{(j)n+1} \otimes \bar{\mathbf{S}}_{(j)n+1} & \text{otherwise} \end{cases} \tag{55}$$

where $\tilde{\mathbf{M}} = \mathsf{P} : \mathbf{M}$. Note that the present formulation results in a symmetric algorithmic tangent modulus Eq. (54) with a low computational cost [49].

Following plasticity nomenclature, further examination of Eqs. (45–49) results in the observation that if $\Phi_j < 0$ or $\Lambda_j < 0$, then no damage or softening evolution takes place with respect to the jth damage or softening surface. Algorithmically, this motivates the notation of a "trial" elastic predictor state defined by $\dot{r}_{j_t} = 0$ for all k or $\dot{\Gamma}_{j_t} = 0$ for all j [24]. The trial stress is given by

$$\sigma_{n+1}^{trial} = p_{n+1}\mathbf{1} + \sum_{j=m,f_1,f_2} \left[1 - D_{j_n}\right] \bar{\sigma}^0_{(j)n+1} \tag{56}$$

the trial damage is given by

$$D^{\alpha\ trial}_{j_{n+1}} = D^{\alpha}_{j_n} \quad \text{and} \quad w^{trial}_{j_{n+1}} = w_{j_n} \tag{57}$$

and the symmetric algorithmic material tensor

$$\mathsf{C}^{\boldsymbol{trial}}_{\boldsymbol{n+1}} = \mathsf{C}^{\boldsymbol{0}}_{\mathrm{vol}\,\boldsymbol{n+1}} + \sum_{\boldsymbol{j=m,f_1,f_2}} \left[\boldsymbol{1} - \boldsymbol{D}_{\boldsymbol{j_n}}\right] \mathsf{C}^{\boldsymbol{0}}_{\boldsymbol{(j)n+1}} \tag{58}$$

A predictor-corrector type algorithmic can now be defined as follows:

1. For each j check whether $\Phi_{j_{n+1}} \leq 0$. If so, then assume the surface is inactive, so $D^{\alpha}_{(j)n+1} = D^{\alpha\ trial}_{(j)n+1}$.
2. If $\Phi_{j_{n+1}} > 0$, then assume that the surface is active and update $D^{\alpha}_{(j)n+1}$ using Eq. (48).
3. For each j check whether $\Lambda_{(j)n+1} \leq 0$. If so, then assume the surface is inactive, so $w_{j_{n+1}} = w^{trial}_{j_{n+1}}$.
4. If $\Lambda_{(j)n+1} > 0$, then assume that the surface is active and update w_j using Eq. (52).

To update softening and damage variables, we summarize the computational algorithm for the case of $\Gamma_{i_{n+1}} = \frac{\partial \Psi_{\mathrm{ich(i)n+1}}}{\partial \Gamma_i}$ and explicit actualization of $w_{i_{n+1}}$ in Table 3.

In this example, we compare the model here presented with experimental stress-stretch data from uniaxial cyclic loading tests on vein tissue [3]. These experiments were developed in our laboratory in order to study the properties of ovine vena cava tissue. Two families of fibers oriented in circumferential (collagen) and longitudinal (elastin) directions were considered. The material is treated as incompressible $\left(\mathbf{C} = \bar{\mathbf{C}}\right)$, with the matrix modelled using the following strain energy

Table 3 Algorithmic procedure and explicit actualization of damage and softening variables

1. Database at each Gaussian point D_{sk_n}, $\Xi_{(k_t)n}$, D_{rk_n}, $\bar{\Psi}^0_{(\mathrm{k})\mathrm{n}}$, w_{i_n}, $\Gamma_{i_{t_n}}$
2. Compute the initial elastic stress tensors ($\sigma^0_{(k)n+1}$) and the initial elastic modulus ($\mathbf{c}^0_{n+1}$)
3. Compute the current equivalent measures

   $\Xi_{k_{n+1}} = \sqrt{2\bar{\Psi}^0_{(\mathrm{k})\mathrm{n}+1}}$ and $\Gamma_{i_{n+1}} = \frac{\partial \bar{\Psi}_{(\mathrm{i})\mathrm{n}+1}}{\partial I'_i}$
4. Check the discontinuous damage criterion

   $\Phi_{k_{n+1}}(\bar{\mathbf{C}}_{n+1}, \Xi_{(k_t)n}) = \sqrt{2\bar{\Psi}^0_{(\mathrm{k})\mathrm{n}+1}} - \Xi_{(k_t)n} = \Xi_{k_{n+1}} - \Xi_{(k_t)n} > 0$

   YES: update discontinuous damage internal variables

   $D_{sk_{n+1}} = \frac{1}{1+\exp(-\alpha_k[\Xi_{k_{n+1}} - \gamma_k])}$

   $\bar{\mathbf{S}}^{s_k}_{(k)n+1} = D'_{sk_{n+1}} \bar{\mathbf{S}}^0_{(k)n+1} \otimes \bar{\mathbf{S}}^0_{(k)n+1}$

   $\Xi_{(k_t)n+1} = \Xi_{k_{n+1}}$

   NO: no additional damage $D_{sk_{n+1}} = D_{sk_n}$ and $\bar{\mathbf{S}}^{s_k}_{(k)n+1} = 0$.
5. Update continuous damage internal variables

   $r_{k_{n+1}} = r_{k_n} + |\bar{\Psi}^0_{(\mathrm{k})\mathrm{n}+1} - \bar{\Psi}^0_{(\mathrm{k})\mathrm{n}}|$.

   $D_{rk_{n+1}} = d^{r_k}_{\infty}\left[1 - \exp\left(-\frac{r_{k_{n+1}}}{\zeta_k}\right)\right]$

   $\bar{\mathbf{S}}^{r_k}_{(k)n+1} = D'_{(rk)n+1} \mathrm{sign}(\dot{f}_{(k)n+1}) \bar{\mathbf{S}}^0_{(k)n+1} \otimes \bar{\mathbf{S}}^0_{(k)n+1}$
6. Check the softening criterion

   $\Lambda_i(\mathbf{C}(t), \Gamma_{i_t}) = \frac{\partial \bar{\Psi}_{(\mathrm{i})}}{\partial I'_i}(\bar{\mathbf{C}}(t), \mathbf{M}, \mathbf{N}) - \Gamma_{i_t} = \Gamma_i - \Gamma_{i_t} \leq 0$

   YES: update softening internal variables

   $w_{i_{n+1}} = \frac{\kappa_i}{I_{i0}} \Gamma_{i_{n+1}} + 1$

   $\bar{\mathbf{S}}^{w_i}_{(i)n+1} = -4J^{-\frac{2}{3}} \frac{\kappa_i}{I_{i0}} \tilde{\Gamma}_i \frac{\partial^2 \bar{\Psi}_{n+1}}{\partial I'_i{}^2_{n+1}} \tilde{\mathbf{M}} \otimes \tilde{\mathbf{M}}$

   $\Gamma_{i_{t_{n+1}}} = \Gamma_{i_{n+1}}$

   NO: no additional damage $w_{i_{n+1}} = w_{i_n}$ and $\bar{\mathbf{S}}^{w_i}_{(i)n+1} = 0$.
7. Compute the Cauchy stress tensor

   $p_{n+1} = \frac{d\Psi_{vol}(J_{n+1})}{dJ}|_{n+1}$

   $\sigma_{n+1} = p_{n+1}\mathbf{1} + \sum_{k=m,f_1,f_2}[1 - D_{k_{n+1}}]\mathrm{dev}(\sigma^0_{(k)n+1})$
8. Compute the extra term of the elastic modulus

   $\bar{\mathbf{S}}_{(k,i)n+1} = \bar{\mathbf{S}}^{s_k}_{(k)n+1} + \bar{\mathbf{S}}^{r_k}_{(k)n+1} + \bar{\mathbf{S}}^{w_i}_{(i)n+1}$
9. Compute the elastic modulus

   $\mathbf{c}_{n+1} = \mathbf{c}^0_{\mathrm{vol}n+1} + \sum_{k=m,f_1,f_2}[1 - D_{k_{n+1}}]\bar{\mathbf{c}}^0_{(k)n+1} - \bar{\mathbf{s}}_{(k)n+1}$ with $\bar{\mathbf{s}}_{(k)n+1} = J^{-1}\chi_*(\bar{\mathbf{S}}_{(k)n+1})$

$$\bar{\Psi}(\bar{\mathbf{C}}, \mathbf{M}, \mathbf{N}, D_j, w_j) = \mu[1 - D_m][\bar{I}_1 - 3] + [1 - D_{f_4}]\frac{k_1}{2k_2}\left[\exp\left(k_2[\bar{I}'_4 - 1]^2\right) - 1\right] + [1 - D_{f_6}]\frac{k_3}{2k_4}\left[\exp\left(k_4[\bar{I}'_6 - 1]^2\right) - 1\right]. \quad (59)$$

Table 4 Material, damage and softening parameters for uniaxial simple tension. μ, k_1, k_3 and ζ_j are in MPa, γ_j is in $MPa^{1/2}$ and other parameters are dimensionless [40]

I	μ 0.029	k_1 0.013	k_2 7.760	λ_{4_0} 1.0	k_3 0.010	k_4 0.972	λ_{6_0} 1.0								
	ϖ_m 33.443	γ_m 0.149	ϖ_{f_4} 0.816	γ_{f_4} 9.313	κ_{f_4} 0.026	ϖ_{f_6} 5.491	γ_{f_6} 0.285	κ_{f_6} 1.372	$d_\infty^{r_m}$ 7.242	ζ_m 0.0	$d_\infty^{r_{f_4}}$ 0.100	ζ_{f_4} 4.645	$d_\infty^{r_{f_6}}$ 0.673	ζ_{f_6} 0.182	R^2 0.979
II	μ 0.01	k_1 0.662	k_2 1.295	λ_{4_0} 1.0	k_3 0.049	k_4 0.036	λ_{6_0} 1.0								
	ϖ_m 3.45	γ_m 0.68	ϖ_{f_4} 0.93	γ_{f_4} 19.3	κ_{f_4} 0.08	ϖ_{f_6} 0.9	γ_{f_6} 12.23	κ_{f_6} 0.3	$d_\infty^{r_m}$ 0.3	ζ_m 1.0	$d_\infty^{r_{f_4}}$ 0.3	ζ_{f_4} 1.0	$d_\infty^{r_{f_6}}$ 0.3	ζ_{f_6} 1.0	R^2 0.874

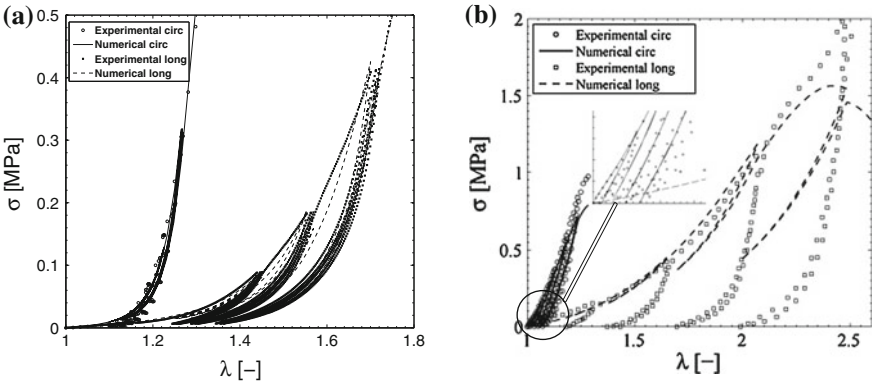

Fig. 7 Experimental and numerical simulation of loading and unloading curves at different load limits in cava tissue [40]. **a** Individual I. **b** Individual II

Table 5 Elastic and damage parameters for the uniaxial test from [47]

μ (kPa)	k_1 (kPa)	k_2 (−)	b (−)	ϖ (−)	γ (kPa)	α (deg)
1.051	286.36	1.40	10.62	0.41	20.10	47.77

μ, k_1 and γ are in MPa, and other parameters are dimensionless

Both pairs of curves—circumferential and longitudinal direction tests for Individuals I and II—were fitted using the representative set of uniaxial data in both axial and circumferential directions with the optimization procedure previously described. The optimized parameters obtained are included in Table 4 and experimental and numerical results for loading and unloading are shown in Fig. 7.

The purpose of this simulation was to present a numerical example of arterial angioplasty with relevance to modeling vascular tissue to demonstrate the capabilities of the model. The model consists of a 10 (mm) length phantom with an external diameter of $D_e = 5$ (mm) and an internal diameter of $D_i = 3.7$ (mm) corresponding to coronary arteries. Only one layer was considered since no experimental data were available for the separates layers and the material parameters are presented in Table 5. The load steps were applied sequentially as follows: (i) Imposition of an initial deformation gradient [4], (ii) Application of an internal pressure of 13.3 (kPa) in the vessel assuming this as the average physiological hemodynamic pressure and (iii) Imposition of pressure to the internal face of the balloon [47] (Fig. 8).

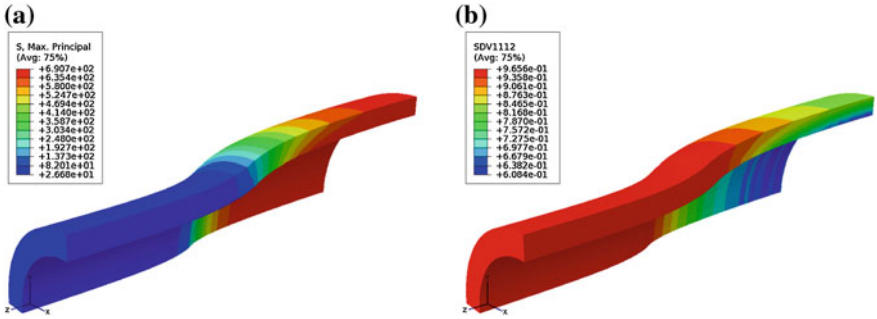

Fig. 8 Stress and average damage at the end of the analysis [47]. **a** Maximal principal Cauchy stress map. **b** Average damage map

5 Conclusions

It is well known that vascular tissues are subject to finite deformations and that their mechanical behavior is highly nonlinear, anisotropic and essentially incompressible with non-zero residual stress and in the non-physiological domain presents viscous and damage behavior and there is significant dispersion in the orientation, which has a significant influence on the mechanical response. The high complexity of biological tissues requires mechanical models that include information of the underlying constituents and look for the physics of the whole processes within the material. This behavior of the micro-constituents can be taken into macroscopic models by means of computational homogenization. It is in this context where the microsphere-based approach acquires high relevance.

In this chapter, we have provided a critical review of the fundamental aspects in modeling this kind of the materials. The application of these constitutive relationships in the context of vascular system has been presented. The increasing effort devoted to studies of mechanical models for soft fibred tissues and the applications aimed at refining basic and clinical analysis demonstrates the vitality of the field of biomechanics [29]. With this approach, a more realistic response of the inelastic evolution is expected due to a smoother transition of the damage in the micro scale. We have limited ourself to an affine model, without taking into account the existing cross-links between fibrils nor the sliding between fibers and matrix [48]. Models presented herein are based on purely passive baseline elasticity. Smooth muscle cells display an important active response, the myogenic tone, which allows the arterial wall to contract or expand acutely to maintain a baseline lumen.

Computational models can help to understand the underlying mechanochemical processes and provide a framework for biological and clinical researchers to jointly enhance the pharmagolocial or surgical management.

Acknowledgments This work was supported by the Spanish Ministry of Economy and Competitiveness (DPI2010-20746-C03-01 and PRI-AIBDE-2011-1216) and the Instituto de Salud Carlos III (ISCIII) through the CIBER initiative and the Plataform for Biological Tissue Characterization of CIBER-BBN. CIBER-BBN is an initiative funded by the VI National R&D&i Plan 2008–2011, Iniciativa Ingenio 2010, Consolider Program, CIBER Actions and financed by the Instituto de Salud Carlos III with assistance from the European Regional Development Fund.

References

1. V. Alastrué, M. A. Martinez, A. Menzel, and M. Doblare. On the use of non-linear transformations for the evaluation of anisotropic rotationally symmetric directional integrals. application to the stress analysis in fibred soft tissues. *Int J Numer Meth Biom Eng*, 79:474–504, 2009.
2. V. Alastrué, M. A. Martínez, M. Doblaré, and A. Menzel. Anisotropic micro-sphere-based finite elasticity applied to blood vessel modelling. *J Mech Phys Solids*, 57:178–203, 2009.
3. V. Alastrué, E. Peña, M. A. Martínez, and M. Doblaré. Experimental study and constitutive modelling of the passive mechanical properties of the ovine infrarenal vena cava tissue. *J Biomech*, 41:3038–3045, 2008.
4. V. Alastrué, J. F. Rodríguez, B. Calvo, and M. Doblaré. Structural damage models for fibrous biological soft tissues. *Int J Solids Struc*, 44:5894–5911, 2007.
5. V. Alastrué, P. Saez, M. A. Martínez, and M. Doblaré. On the use of bingham statistical distribution in microsphere-based constitutive models fo arterial tissue. *Mech Res Commun*, 37:700–706, 2010.
6. E. M. Arruda and M. C. Boyce. A three-Ddimensional constitutive model for the large stretch behavior of rubber elastic materials. *J Mech Phys Solids*, 41:389–412, 1993.
7. C. Bingham. An antipodally summetric distribution on the sphere. *Ann Stat*, 2:1201–1225, 1974.
8. J. Bonet and R. D. Wood. *Nonlinear Continuum Mechanics for Finite Element Analysis*. Cambridge University Press, Cambridge, 2008.
9. B. Calvo, E. Peña, P. Martins, T. Mascarenhas, M. Doblare, R. Natal, and A. Ferreira. On modelling damage process in vaginal tissue. *J Biomech*, 42:642–651, 2009.
10. B. Calvo, E. Peña, M. A. Martínez, and M. Doblaré. An uncoupled directional damage model for fibered biological soft tissues. Formulation and computational aspects. *Int J Numer Meth Engng*, 69:2036–2057, 2007.
11. P. B. Canham, H. M. Finlay, and D. R. Boughner. Contrasting structure of the saphenous vein and internal mammary artery used as coronary bypass vessels. *Cardiovasc Res*, 34:557–567, 1997.
12. P. B. Canham, H. M. Finlay, J. G. Dixon, D. R. Boughner, and A. Chen. Measurements from light and polarised light microscopy of human coronary arteries fixed at distending pressure. *Cardiovasc Res*, 23:973–982, 1989.
13. H. Demiray, H. W. Weizsacker, K. Pascale, and H. Erbay. A stress-strain relation for a rat abdominal aorta. *J Biomech*, 21:369–374, 1988.
14. K.P. Dingemans, P. Teeling, J. H. Lagendijk, and A. E. Becker. Extracellular matrix of the human aortic media: an ultrastructural histochemical and immunohistochemical study of the adult aortic media. *Anat Rec*, 258:1–14, 2000.
15. H. M. Finlay, L. McCullough, and P. B. Canham. Three-dimensional collagen organization of human brain arteries at different transmural pressures. *J Vasc Res*, 32:301–312, 1995.
16. P. J. Flory. Thermodynamic relations for high elastic materials. *Trans Faraday Soc*, 57:829–838, 1961.

17. Y. C. Fung, K. Fronek, and P. Patitucci. Pseudoelasticity of arteries and the choice of its mathematical expression. *Am J Physiol*, 237:H620–H631, 1979.
18. A. García. *Experimental and numerical framework for modelling vascular diseases and medical devices*. PhD thesis, University of Zaragoza, Spain, Division of Solids and Structural Mechanics, 2012.
19. A. García, M. A. Martínez, and E. Peña. Determination and Modeling of the Inelasticity Over the Length of the Porcine Carotid Artery. *ASME J Biomech Eng*, 135:031004–1, 2013.
20. A. García, E. Peña, A. Laborda, F. Lostalé, M. A. De Gregorio, M. Doblaré, and M. A. Martínez. Experimental study and constitutive modelling of the passive mechanical properties of the porcine carotid artery and its relation to histological analysis. Implications in animal cardiovascular device trials. *Med Eng Phys*, 33:665–676, 2011.
21. A. García, E. Peña, and M. A. Martínez. Viscoelastic properties of the passive mechanical behavior of the porcine carotid artery: Influence of proximal and distal positions. *Biorheology*, 49:271–288, 2012.
22. P. Sáez, A. García, E. Peña, T.C. Gasser and M. A. Martínez. Microstructural analysis of fiber orientation in swine carotid artery: structural quantification and constitutive modelling. *Submitted*, 2015.
23. T. C. Gasser, R. W. Ogden, and G. A. Holzapfel. Hyperelastic modelling of arterial layers with distributed collagen fibre orientations. *J R Soc Interface*, 3:15–35, 2006.
24. S. Govindjee, G. J. Kay, and J. C. Simo. Anisotropic modelling and numerical simulation of brittle damage in concrete. *Int J Numer Meth Engng*, 38:3611–3633, 1995.
25. C. S. Herz. Bessel functions of matrix argument. *Ann Math*, 61:474–523, 1955.
26. G. A. Holzapfel, T. C. Gasser, and R. W. Ogden. A new constitutive framework for arterial wall mechanics and a comparative study of material models. *J Elasticity*, 61:1–48, 2000.
27. G. A. Holzapfel, T. C. Gasser, and M. Stadler. A structural model for the viscoelastic behaviour of arterial walls: Continuum formultaion and finite element analysis. *Eur J Mech A/ Solids*, 21:441–463, 2002.
28. G. A. Holzapfel and R. W. Ogden. Constitutive modelling of passive myocardium: a structurally based framework for material characterization. *Phil Trans R Soc A*, 367:3445–3475, 2009.
29. G. A. Holzapfel and R. W. Ogden. Constitutive modelling of arteries. *Phil Trans R Soc A*, 466:1551–1597, 2010.
30. E. W. Hsu, A. L. Muzikant, S. A. Matulevicius, R. C. Penland, and C. S. Henriquez. Magnetic resonance myocardial fiber-orientation mapping with direct histological correlation. *Am J Physiol HeartCirc Physiol*, 274:H1627–H1634, 1998.
31. J. D. Humphrey. Mechanics of the arterial wall: Review and directions. *Crit Rev Biomed Eng*, 23:1–162, 1995.
32. J. W. Ju. On energy-based coupled elastoplastic damage theories: Constitutive modeling and computational aspects. *Int J Solids Struct*, 25:803–833, 1989.
33. Y. Lanir. A structural theory for the homogeneous biaxial stress-strain relationship in flat collageneous tissues. *J Biomech*, 12:423–436, 1979.
34. Y. Lanir. Constitutive equations for fibrous connective tissues. *J Biomech*, 16:1–12, 1983.
35. E. Maher, M. Early, A. Creane, C Lally, and D. J. Kelly. Site specific inelasticity of arterial tissue. *J Biomech*, 45:1393–1399, 2012.
36. D. W. Marquardt. An algorithm for least-squares estimation of nonlinear parameters. *Siam J Appl Math*, 11:431–441, 1963.
37. J. E. Marsden and T. J. R. Hughes. *Mathematical Foundations of Elasticity*. Dover, New York, 1994.
38. E. Peña. ". Application to soft biological tissues. *Comp Mech*, 48:407–420, 2011.
39. E. Peña. Prediction of the softening and damage effects with permanent set in fibrous biological materials. *J Mech Phys Solids*, 59:1808–1822, 2011.
40. E. Peña. Computational aspects of the numerical modelling of softening, damage and permanent set in soft biological tissues. *Comput Struct*, 130:57–72, 2014.

41. E. Peña, V. Alastrue, A. Laborda, M. A. Martínez, and M. Doblare. A constitutive formulation of vascular tissue mechanics including viscoelasticity and softening behaviour. *J Biomech*, 43:984–989, 2010.
42. E. Peña, A. Pérez del Palomar, B. Calvo, M. A. Martínez, and M. Doblaré. Computational modelling of diarthrodial joints. Physiological, pathological and pos-surgery simulations. *Arch Comput Method Eng*, 14(1):47–91, 2007.
43. E. Peña, P. Martins, T. Mascarenhas, R. M. Natal-Jorge, A. Ferreira, M. Doblaré, and B. Calvo. Mechanical characterization of the softening behavior of human vaginal tissue. *J Mech Behav Biomed*, 4:275–283, 2011.
44. E. Peña, J. A. Peña, and M. Doblaré. On the Mullins effect and hysteresis of fibered biological materials: A comparison between continuous and discontinuous damage models. *Int J Solids Struct*, 46:1727–1735, 2009.
45. J. F. Rodríguez, V. Alastrue, and M. Doblaré. Finite element implementation of a stochastic three dimensional finite-strain damage model for fibrous soft tissue. *Comput Methods Appl Mech Engrg*, 197:946–958, 2008.
46. J. F. Rodríguez, F. Cacho, J. A. Bea, and M. Doblaré. A stochastic-structurally based three dimensional finite-strain damage model for fibrous soft tissue. *J Mech Phys Solids*, 54:564–886, 2006.
47. P. Sáez, V. Alastrué, E. Peña, M. Doblaré, and M. A. Martínez. Anisotropic microsphere-based approach to damage in soft fibered tissue. *Biomechan Model Mechanobiol*, 11:595–608, 2012.
48. P. Sáez, E. Peña, and M. A. Martínez. A structural approach including the behavior of collagen cross-links to model patient-specific human carotid arteries. *Ann Biomed Eng*, 42:1158–1169, 2014.
49. J. C. Simo. On a fully three-dimensional finite-strain viscoelastic damage model: Formulation and computational aspects. *Comput Methods Appl Mech Engrg*, 60:153–173, 1987.
50. J. C. Simo and J. W. Ju. Strain- and stress-based continuum damage models. I. Formulation. *Int J Solids Struct*, 23:821–840, 1987.
51. J. C. Simo and J. W. Ju. Strain- and stress-based continuum damage models. II. Computational aspects. *Int J Solids Struct*, 23:841–870, 1987.
52. J. C. Simo, R. L. Taylor, and K. S. Pister. Variational and projection methods for the volume constraint in finite deformation elasto-plasticity. *Comput Methods Appl Mech Engrg*, 51:177–208, 1985.
53. J. F. Smith, P. B. Canham, and J. Starkey. Orientation of collagen in the tunica adventitia of the human cerebral artery measured with polarized light and the universal stage. *J Ultrastruct Res*, 77:133–45, 1981.
54. D. P. Sokolis. A passive strain-energy function for elastic and muscular arteries: correlation of material parameters with histological data. *Med Biol Eng Comput*, 48:507–518, 2010.
55. A. J. M. Spencer. Theory of Invariants. In *Continuum Physics*, pages 239–253. Academic Press, New York, 1971.
56. K. Takamizawa and K. Hayashi. Strain-Energy Density-Function and Uniform Strain Hypothesis for Arterial Mechanics. *J Biomech*, 20:7–17, 1987.
57. A. Tobolsky, I. Prettyman, and J Dillon. Stress relaxation of natural and synthetic rubber stocks. *J Appl Phys*, 15:380–395, 1944.
58. C.N. van den Broek, A. van der Horst, M. C. M. Rutten, and F. N. van de Vosse. A generic constitutive model for the passive porcine coronary artery. *Biomech Mod Mechanobiol*, 10:249–258, 2011.
59. J. A. Weiss, B. N. Maker, and S.Govindjee. Finite element implementation of incompressible, transversely isotropic hyperelasticity. *Comput Methods Appl Mech Engrg*, 135:107–128, 1996.
60. A. S. Wineman and K. R. Rajagopal. On a constitutive theory for materials undergoing microstructural changes. *Arch Mech*, 42:53–75, 1990.
61. R. Wulandana and A. M. Robertson. An inelastic multi-mechanism constitutive equation for cerebral arterial tissue. *Biomech Model Mechanbiol*, 4:235–248, 2005.

62. M. Zullinger, P. Fridez, K. Hayashi, and N. Stergiopulos. A strain energy function for arteries accounting for wall composition and structure. *J Biomech*, 37:989–1000, 2004.
63. M. Zullinger, A. Rachev, and N. Stergiopulos. A constitutive formulation of arterial mechanics including vascular smooth muscle tone. *Am J Physiol Heart Circ Physiol*, 287:H1335–H1343, 2004.

http://www.springer.com/978-3-319-15798-6

Computational and Experimental Biomedical Sciences:
Methods and Applications
ICCEBS 2013 -- International Conference on
Computational and Experimental Biomedical Sciences
Tavares, J.M.R.S.; Natal Jorge, R.M. (Eds.)
2015, XV, 259 p. 116 illus., Hardcover
ISBN: 978-3-319-15798-6